Proceedings of ASME Turbo Expo 2012
GT2012
June 11-15, 2012, Copenhagen, Denmark

GT2012-69412

INFLUENCES ON THE OIL SPLIT BETWEEN THE OFFTAKES OF AN AERO-ENGINE BEARING CHAMBER

Wolfram Kurz*, Klaus Dullenkopf, Hans-Jörg Bauer
Institut für Thermische Strömungsmaschinen
Karlsruhe Institute of Technology (KIT)
76131 Karlsruhe, Germany

ABSTRACT

The aim of the presented work was to identify factors that influence the oil split between the two offtakes of a vented aero-engine bearing chamber. The impact of different vent and scavenge offtake designs was experimentally investigated with a test rig at the ITS. The generic bearing chamber was also equipped with ten film thickness sensors. The film measurements allowed a further evaluation of the mechanisms behind different oil splits. Two of the examined offtake features ensured a very constant oil split: a protruding vent and a covered ramp offtake. The latter also decreased the oil film thickness on the bearing chamber walls significantly. Furthermore, an influence of a non-uniform seal gap was detected which altered the oil split by several percent.

NOMENCLATURE

$\dot{V}$	Volume flow rate
$\dot{m}$	Mass flow rate
n	Shaft speed
d	Diameter
r	Radius
b	Width
h	Height
K	Film thickness correction factor
l_{pr}	Protrusion depth
T	Temperature
p	Absolute pressure
η_{sc}	Scavenge efficiency
SR	Scavenge ratio
e	Rotor-stator eccentricity
φ	Angular position

Indices

vt	Vent
sc	Scavenge
l	Oil
g	Air
$seal$	Labyrinth seal
sh	shaft
in	Inflow

INTRODUCTION

An aero-engine bearing chamber contains the oil after its passage through the bearing and returns it to the oil circuit of the engine. If a labyrinth seal is used to seal the bearing chamber, a vent offtake is usually provided for the sealing air and a scavenge offtake for the oil return. The simultaneous presence of air and oil together with a fast rotating shaft, however, causes a complex two-component two-phase flow consisting of wall films, oil droplets and ligaments. As one result, oil also exits through the vent offtake. As the pressure loss of an air/oil two-phase flow in a pipe highly changes with the respective volume flow rates, the anticipation of the oil split between the offtakes is essential for a reliable dimensioning of the oil and secondary air system. Unfortunately, very little is known about factors affecting the oil split. In current designs, more than half of the oil may leave the bearing chamber with the vented air, which requires a high safety

*Corresponding author: wolfram.kurz@kit.edu

Copyright © 2012 by ASME

Downloaded From: http://proceedings.asmedigitalcollection.asme.org/pdfaccess.ashx?url=/data/conferences/asmep/74816/ on 05/01/2017 Terms of Use: http://www.asme.org/abo

factor on the vent air flow to prevent blockage of the vent pipe. As a consequence, more air than needed for sealing is used which reduces engine performance. Therefore, better knowledge of the influences of design features and operating conditions on the oil split in a vented bearing chamber is required.

In the past years, the focus lay on the experimental determination of the prevailing physical effects in a bearing chamber such as oil film thickness [1–3], heat transfer [4–6], droplet generation [7,8] and air flow structures [9]. The schematic in figure 1 summarizes the basic two-phase flow phenomena in a vented bearing chamber. More recent publications [10, 11] concentrated on the two-phase flow in generic scavenge offtakes. [12] were the first to systematically investigate a variation of the scavenge offtake in an engine-typical condition. Water was used as liquid in a ventless arrangment. The influence of geometry variations was assessed by measuring the liquid residence volume. One parameter examined was the scavenge ratio SR which relates the scavenged volume flow to the oil flow rate:

$$SR = \frac{\dot{V}_{sc}}{\dot{V}_{l,in}} = \frac{\dot{V}_{l,sc} + \dot{V}_{g,sc}}{\dot{V}_{l,in}}. \quad (1)$$

While in a ventless bearing chamber $\dot{V}_{l,in} = \dot{V}_{l,sc}$, the oil flow in a vented bearing chamber splits between vent and scavenge offtake: $\dot{V}_{l,in} = \dot{V}_{l,sc} + \dot{V}_{l,vt}$. The same test rig was used by [13] to perform film thickness measurements in an academic configuration. The first investigation discussing oil splits in a vented bearing chamber was presented by [14] where the scavenge efficiency

$$\eta_{sc} = \frac{\dot{V}_{l,sc}}{\dot{V}_{l,in}} = \frac{\dot{V}_{l,sc}}{\dot{V}_{l,sc} + \dot{V}_{l,vt}}. \quad (2)$$

is introduced to describe the oil split between two offtakes and examined for three scavenge offtakes. Besides the experimental approaches, more and more numerical work was published in recent years such as [11, 15–19]. In order to further develop suitable numerical models, more experimental data is needed for validation and for a better understanding of the relevant physical effects.

The study described here represents partly a continuation of the work presented by [14]. The same test rig was used, but the test matrix was extended both with more operating conditions and, more importantly, with more offtake designs. The objectives of the investigation are to (1) determine the oil split for different offtake design configurations and for varying operating conditions, (2) examine the influence of a non-uniform seal clearance, (3) associate the oil split results with film thickness measurements in order to (4) identify the parameters with the highest influence on the two-phase flow in a bearing chamber.

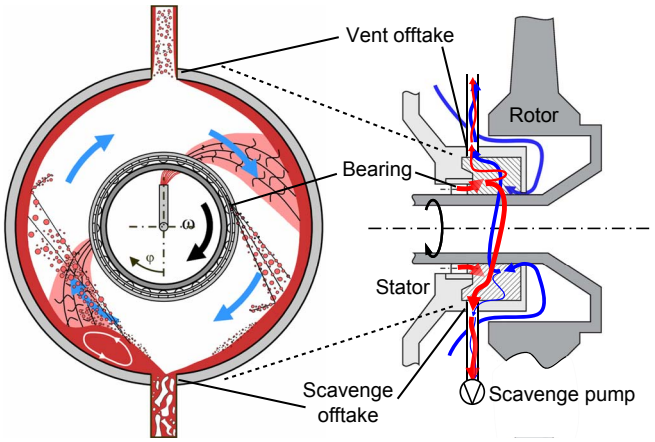

FIGURE 1. TWO-PHASE FLOW PHENOMENA IN AERO-ENGINE BEARING CHAMBERS (left image from [8])

EXPERIMENTAL SETUP

Test rig

In real engine applications there is a large variety of bearing chamber designs and arrangements. For this investigation, the number of variables was limited by imposing the following conditions:

1. Bearing type and dimension: cylindrical roller bearing, inner diameter $d_i = 120\,\text{mm}$, outer diameter $d_o = 152\,\text{mm}$
2. Bearing chamber dimension: $r_{sh} = 64\,\text{mm}$, $b = 66\,\text{mm}$, $h = 47\,\text{mm}$
3. Sealing type: labyrinth seal
4. Vented bearing chamber
5. Offtakes in radial direction and axially centered
6. Fluid temperature $T_g = T_l = 373\,\text{K}$
7. Chamber pressure $p = 2.7\,\text{bar}$
8. No air cross flow over bearing: $\dot{m}_{g,in} = \dot{m}_{g,seal} = \dot{m}_{g,vt} + \dot{m}_{g,sc}$
9. Scavenge ratio $SR = 4$

The influences of the remaining parameters were examined with experiments on the high speed bearing chamber test rig at the *Institut für Thermische Strömungsmaschinen*:

1. Vent and scavenge offtakes: design and angular position
2. Operating conditions: oil flow rate $\dot{V}_{l,in}$, sealing air flow rate $\dot{m}_{g,seal}$, shaft speed n
3. Labyrinth seal clearance

The test rig is depicted in figure 2. Consisting of a high speed shaft, two bearing chambers adjacent to a cylindrical roller bearing, an independent supply of heated air and of heated engine oil (*Mobil Jet Oil II*) and a scavenge pump the test rig allows simulation of aero-engine representative bearing chamber conditions. Most of the published experimental work about bearing chambers [1–9,14] is based on experiments with this highly modular test rig. Figure 3 shows a sectional view of the test rig as it

Copyright © 2012 by ASME

Downloaded From: http://proceedings.asmedigitalcollection.asme.org/pdfaccess.ashx?url=/data/conferences/asmep/74816/ on 05/01/2017 Terms of Use: http://www.asme.org/abo

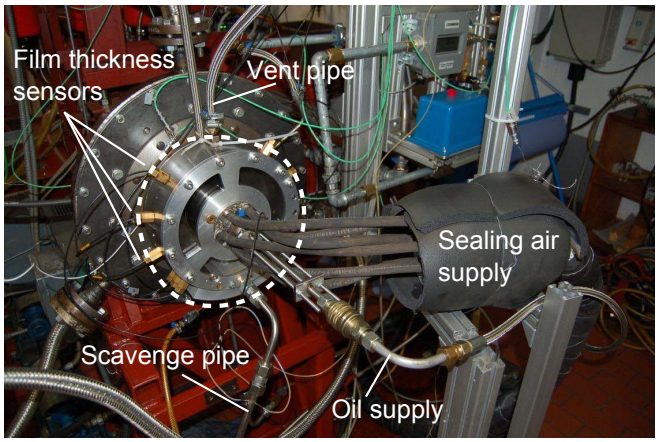

FIGURE 2. THE BEARING CHAMBER TEST RIG

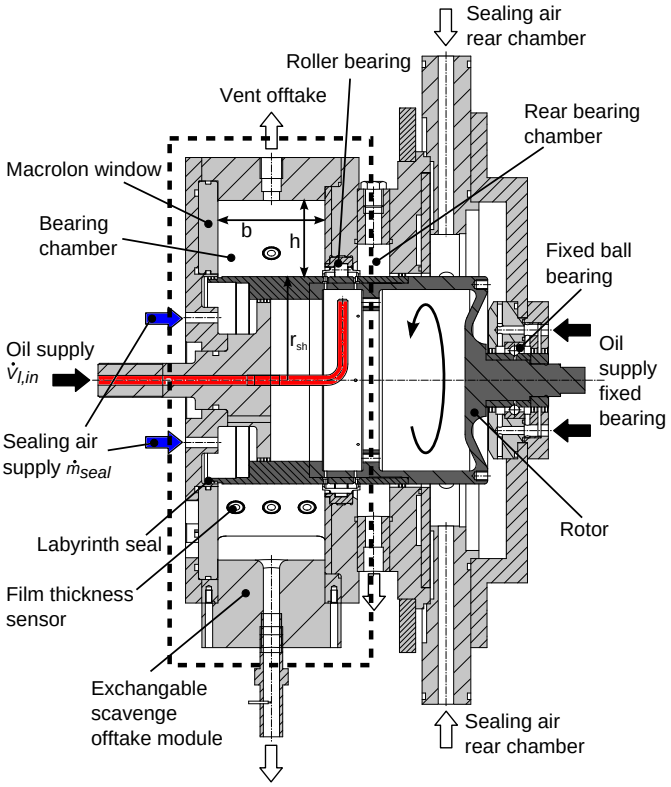

FIGURE 3. SECTIONAL VIEW OF THE TEST RIG

was set up for this investigation. The dashed line highlights the relevant part of the test rig. Oil is supplied to the bearing via under-cage lubrication. Sealing air enters the bearing chamber through a laybrinth seal. Two separator units, one for each offtake flow, capture the oil flow and measure it at the same time. The air flow rates in both vent ($\dot{m}_{g,vt}$) and scavenge pipe ($\dot{m}_{g,vt}$) are also measured independently after separation. In order to fullfill the condition that no air flows across the bearing, automatically controled valves assured the balance

$$\dot{m}_{g,seal} = \dot{m}_{g,vt} + \dot{m}_{g,sc}. \quad (3)$$

Generally, a high degree of automation was necessary for controlling the test rig as the pressure losses in the various pipes strongly changed with the oil split, which required a constant adaption of the valve positions.

In order to quantifiy the oil split, the scavenge efficiency was applied as introduced by [14] , which is directly calculated with the measured oil flows in the vent and scavenge pipe (equation 2). Design variations of the scavenge offtake were achieved by inserting different modules that were placed in a 70°-cut in the lower part of the chamber. The vent offtake consisted of a threaded piece of pipe that could be mounted either flush or protruding up to 10 mm into the chamber. Figure 6 depicts the positions of the film thickness sensors with three sensors at position $\varphi = 135°$ as can be seen in figure 3. As the thread of the film thickness sensor mounts is the same as of the vent offtake mount, it can be placed at any position of a film thickness sensor and vice versa. Furthermore, a viewing window allowed direct visual observation of the two-phase flow in the bearing chamber to support the interpretation of the measured data.

Film thickness measurement technique

The principle of the applied film thickness measurement technique is schematically depicted in figure 4: As the oil has a higher relative permittivity than air the capacitance above the sensor changes with the height of the oil film. In order to prevent any disturbance of the oil film by the sensor, each sensor was equipped with a small polycarbonate platelet which was polished after the assembly of the sensor to fit the surface of the housing. An in-situ calibration of each sensor was then performed using adhesive tape which has a relative permittivity similar to hot engine oil. Correcting the voltage output signal from the adhesive tape calibration by a constant, experimentally determined factor K yielded the calibration curve for hot engine oil (figure 4). Before starting an experiment with air and oil flows, it was necessary to measure the offset voltage of the hot, dry sensor as the capacitance of the platelet is also temperature dependent. This way individually and in-situ calibrated, the capacitive sensors allowed a robust film thickness measurement in this hot and vibrating environment.

Copyright © 2012 by ASME

Downloaded From: http://proceedings.asmedigitalcollection.asme.org/pdfaccess.ashx?url=/data/conferences/asmep/74816/ on 05/01/2017 Terms of Use: http://www.asme.org/abo

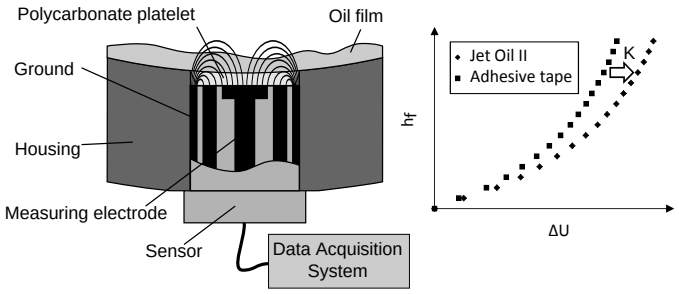

FIGURE 4. DETERMINATION OF FILM THICKNESS USING CAPACITIVE SENSORS (ADAPTED FROM [3])

TABLE 1. MEASUREMENT UNCERTAINTIES

$\dot{V}_{l,in}$	$\dot{m}_{g,seal}$	n	T	p	SR
$\pm 14\,\%$	$\pm 4\,\%$	$\pm 0.5\,\%$	$\pm 2\,\%$	$\pm 6\,\%$	$\pm 12\,\%$

Estimation of measurement uncertainties

The precision of the averaged film thickness values was calculated to be better than $\pm 0.05\,\text{mm}$. The accuracy of the film thickness measurement technique was estimated with a sensitivity analysis. Uncertainties can arise from three factors: the calibration with adhesive tape, the correction factor K and the offset voltage of the hot sensor. A repetitive calculation of the averaged film thickness values based on all combinations of the upper and lower limits of these factors yields a maximum and minimum averaged film thickness value for each sensor. The error bars in the figures 14 - 16 indicate these measurement uncertainties which are smaller than 21 % of the measured value. A similar accuracy range for this measurement technique was also estimated by [20]. An unknown uncertainty is the content of air dispersed in the oil film. Although the sensing surface is 10 mm in diameter, this spatial averaging effect is secondary as the values were also time-averaged.

The uncertainties of the parameters that define an operating point, the oil flow $\dot{V}_{l,in}$, the sealing air flow $\dot{m}_{g,seal}$, the shaft speed n, the chamber temperature T, the chamber pressure p and the scavenge ratio SR are given in table 1 (95 % confidence). The uncertainty of the calculated scavenge efficiency η_{sc} depends on the uncertainties of the independent oil flow measurements $\dot{V}_{sc}$ and $\dot{V}_{vt}$ which are estimated to be around $\pm 10\,\%$ of the measured value. The error bars in the figures 7 and 9 - 13 represent the resulting uncertainty, which was calculated for each measuring point following the procedure given in [21].

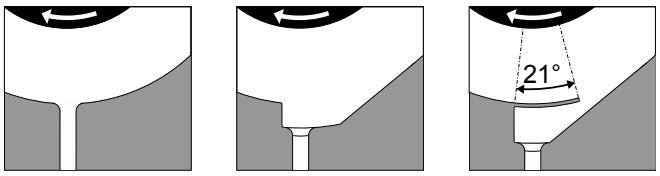

(a) BASELINE **(b)** SHALLOW RAMP WITHOUT COVER **(c)** DEEP RAMP WITH 21° COVER

FIGURE 5. SCHEMATICS OF THE SCAVENGE OFFTAKES

Examined features

Scavenge design From the immense variety of possible configurations, two basic scavenge designs were chosen (figure 5): a rounded hole offtake served as baseline configuration and a ramp offtake which is supposed to guide the oil film better towards the offtake pipe. In addition, the ramp insert allowed examination of the influence of the ramp depth by setting a shallow ramp with $r_{ramp}/(r_{sh}+h) = 1.14$ or a deeper ramp with $r_{ramp}/(r_{sh}+h) = 1.22$. A further design variation was achieved by covering a certain segment of the ramp (0°, 6°, 12° and 21°). Both additional inserts are depicted in figure 6.

Vent design The vent offtake variations were tested with the baseline scavenge design as it promised to show the clearest change of oil split. A combination of a protrusion depth variation from $l_{pr} = 0\,\text{mm}$ (flush mount, see figure 6) to $l_{pr} = 10\,\text{mm}$ with four angular positions yielded nine test points.

Operating conditions The interaction between the operating parameters oil flow $\dot{V}_{l,in}$, sealing air flow $\dot{m}_{g,seal}$ and shaft speed n was examined for two offtakes: (1) the baseline offtake as reference which showed the strongest variations of oil split and (2) the 21 ° covered ramp configuration with the highest scavenge efficiency of all ramp designs (see figure 5(c)). Air and oil flows were varied according to the test matrix given in table 2. The shaft speed was varied in steps of 5,000 rpm from $n = 2,500\,\text{rpm}$ to $n = 15,000\,\text{rpm}$ for each test point. As the oil split showed always the largest differences at the highest shaft speed, the influences of the other features will be discussed at $n = 15,000\,\text{rpm}$ and at reference point (RP) conditions.

Labyrinth seal clearance Particular care was taken to precisely position the front cover of the bearing chamber, which contains the viewing window and forms the counter part to the labyrinth seal. As an eccentric position of the cover leads to a non-uniform sealing gap, three tests at the reference condition were carried out. A possible rotor/stator eccentricity e leads to a non uniform sealing clearance with a minimum value of $h_{seal,min} = h_{seal} - e$ and a maximum value of $h_{seal,max} = h_{seal} + e$.

Copyright © 2012 by ASME

Downloaded From: http://proceedings.asmedigitalcollection.asme.org/pdfaccess.ashx?url=/data/conferences/asmep/74816/ on 05/01/2017 Terms of Use: http://www.asme.org/abo

TABLE 2. TEST MATRIX. *RP*: REFERENCE POINT

#	$\dot{V}_{l,in}$ [l/h]	$\dot{m}_{g,seal}$ [g/s]	$T_g = T_l$ [K]	p [bar]	SR [-]
1	50	5.0			
2	50	15.0			
3	150	5.0	373	2.7	4
4	150	15.0			
RP	100	10.0			

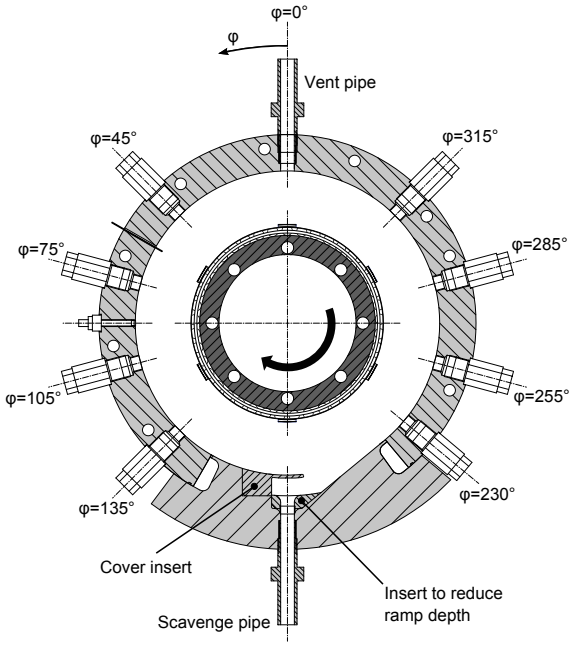

FIGURE 6. POSITIONS OF FILM THICKNESS SENSORS; CONFIGURATION WITH A COVERED SHALLOW RAMP AND A FLUSH MOUNTED VENT OFFTAKE

The position of the maximum and minimum clearance depends on the angular position of the eccentricity. Two cases were considered: the maximum clearance at $\varphi = 90^\circ$ and at $\varphi = 270^\circ$.

RESULTS AND DISCUSSION

Oil Split

Baseline Offtake Figure 7 shows the scavenge efficiency against shaft speed for the baseline scavenge offtake configuration at the reference point conditions (table 2). The vent offtake was flush mounted. With increasing shaft speed, more

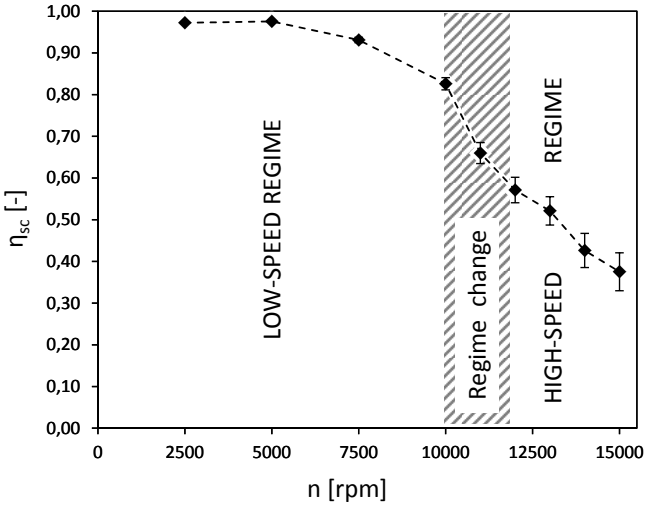

FIGURE 7. OIL SPLIT FOR THE BASELINE CONFIGURATION

and more oil left the bearing chamber through the vent port. This was the case for almost every configuration. With increasing shaft speeds gravity becomes less important. The question where the oil leaves the chamber depends then more and more on the suction capacity of the two offtakes, which is considerably higher in the case of the vent offtake: At the reference point the vented mass flow of air of $\dot{m}_{g,vt} = 10\,\mathrm{g/s}$ corresponds to approximately $\dot{V}_{g,vt} = 14{,}000\,\mathrm{l/h} \gg \dot{V}_{g,sc}(n = 15{,}000\,\mathrm{rpm}) \approx 363\,\mathrm{l/h}$.

Furthermore, two different two-phase flow regimes were visually detected: a low-speed regime and a high-speed regime. The photographs through the viewing front window depicted in figure 8 give an impression of the two regimes. The low-speed regime is characterized by a rezirculation zone at the bottom of the chamber. At a certain shaft speed the flow appearance suddenly changed to the high-speed regime which appeared to be dominated by the rotating air flow. Also, the scavenge efficiency dropped particularly after the flow had changed to the high-speed regime (figure 7). The shaft speed at which the flow regime changed was not constant for all tested configurations. It depended on sealing air flow, oil flow and offtake configuration. A detailed discussion of this phenomenon would go beyond the scope of this work, but will be part of a future publication.

Figure 9 depicts the scavenge efficiency of the same baseline configuration, but for the flow conditions as given in table 2. The overall tendency is always a decreasing scavenge efficiency for increasing rotational speed. A higher sealing air flow further decreases the scavenge efficiency. Note that although the same scavenge efficiency was determined for $\dot{V}_{l,in} = 50\,\mathrm{l/h}$ and $\dot{V}_{l,in} = 150\,\mathrm{l/h}$ at $\dot{m}_{g,seal} = 15.0\,\mathrm{g/s}$, the respective overall oil flow rates in the vent $\dot{V}_{l,vt}$ are $39\,\mathrm{l/h}$ and $118\,\mathrm{l/h}$ due to the different total oil flow rates $\dot{V}_{l,in}$.

Copyright © 2012 by ASME

Downloaded From: http://proceedings.asmedigitalcollection.asme.org/pdfaccess.ashx?url=/data/conferences/asmep/74816/ on 05/01/2017 Terms of Use: http://www.asme.org/abo

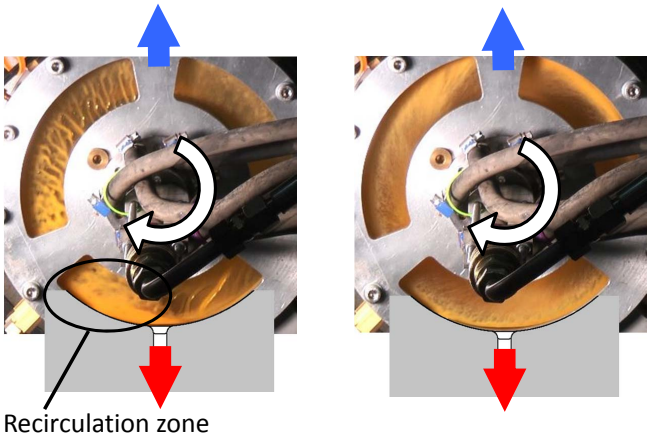

(a) LOW-SPEED REGIME (b) HIGH-SPEED REGIME

FIGURE 8. TWO-PHASE FLOW REGIMES IN THE EXAMINED BEARING CHAMBER

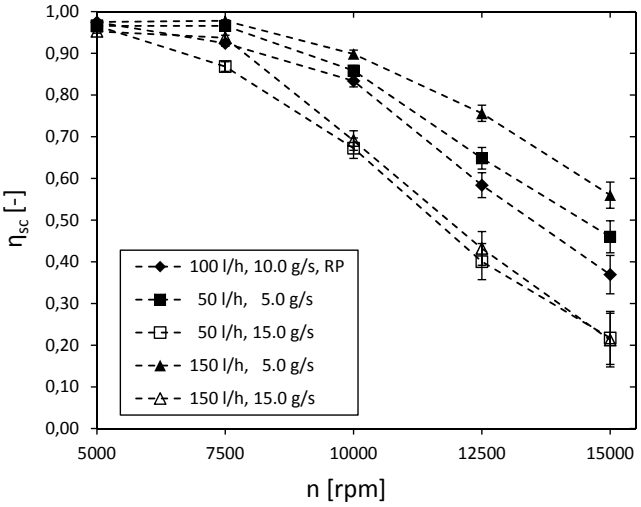

FIGURE 9. BASELINE: OIL SPLIT VS. SHAFT SPEED FOR DIFFERENT COMBINATIONS OF $\dot{V}_{l,in}$ AND $\dot{m}_{g,seal}$

Ramp Offtake As the highest changes of scavenge efficiency occured at 15,000 rpm, the influences of the different scavenge offtake features are discussed at this shaft speed and at reference point conditions (table 2). Figure 10 gives an overview over the oil split for different ramp configurations. The baseline oil split serves as a reference. The deep ramp showed always a higher η_{sc} than the shallow ramp. Inserting a cover further increased the efficiency, as it reduces the influence of the rotating air flow on the scavenge offtake. The use of a deep ramp with the 21° cover, which almost closes the ramp cut (figure 5(c)), pushed the scavenge efficiency from 39 % up to 88 %. Therefore, it was also subjected to the variation of operating conditions

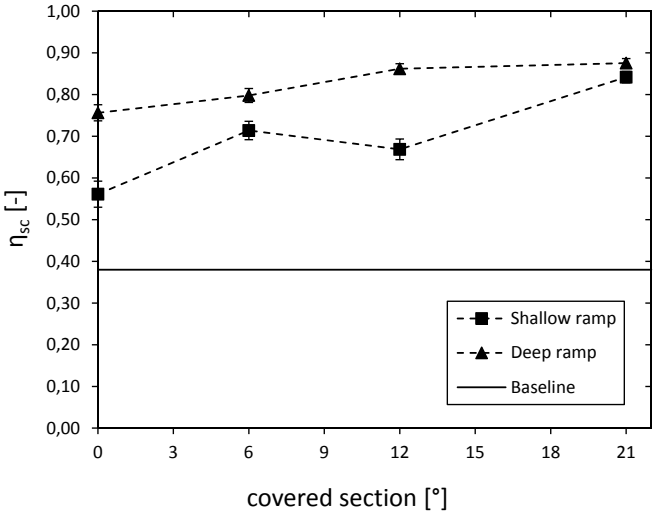

FIGURE 10. RAMP: η_{sc} AT 15,000 rpm FOR A DEEP AND A SHALLOW RAMP VS. COVER LENGTH

like the baseline case. The results are shown in figure 11. This design not only keeps η_{sc} at a high level (above 77 %) for all examined flow conditions, but the fluctuations are also smaller. Furthermore, the covered ramp offtake showed a minimum of η_{sc} at 12.500 rpm followed by a slight increase at 15,000 rpm for low sealing air and oil flows ($\dot{V}_{l,in} = 50\,^{l}/_{h}, \dot{m}_{g,seal} = 5.0\,^{g}/_{s}$ and $\dot{V}_{l,in} = 100\,^{l}/_{h}, \dot{m}_{g,seal} = 10.0\,^{g}/_{s}$), which is contrary to the usually observed uniform decrease of η_{sc} like in the baseline case. Further investigations are necessary to understand the reasons for this behaviour. An explanation could be that due to the good scavenge performance of this offtake, the oil film might be mostly responsible for the amount of oil in the vent. As the oil film is faster due to the increased shaft speed, less oil is sucked into the vent offtake at the higher shaft speed.

Vent protrusion and position The oil split results for the vent variations are depicted in figure 12, again at 15,000 rpm. A protruding vent turned out to be a very effective measure to increase η_{sc}, as it prevents the oil film from directly being sucked into the vent pipe. Displacing the vent in the direction of shaft rotation (arrow indicates direction of shaft surface velocity) also slightly increased η_{sc}. The explanation is as for the above discussed covered ramp case: the oil film has a higher momentum than at the top position and is therefore more likely to pass the vent which results in less oil in the vent.

Non-uniform seal clearance The nominal labyrinth seal clearance in the test rig was $h_{seal} = 0.7$ mm. In order to ensure a uniform inflow of sealing air, the front cover plate was carefully assembled by measuring and setting the position with

Copyright © 2012 by ASME

Downloaded From: http://proceedings.asmedigitalcollection.asme.org/pdfaccess.ashx?url=/data/conferences/asmep/74816/ on 05/01/2017 Terms of Use: http://www.asme.org/abo

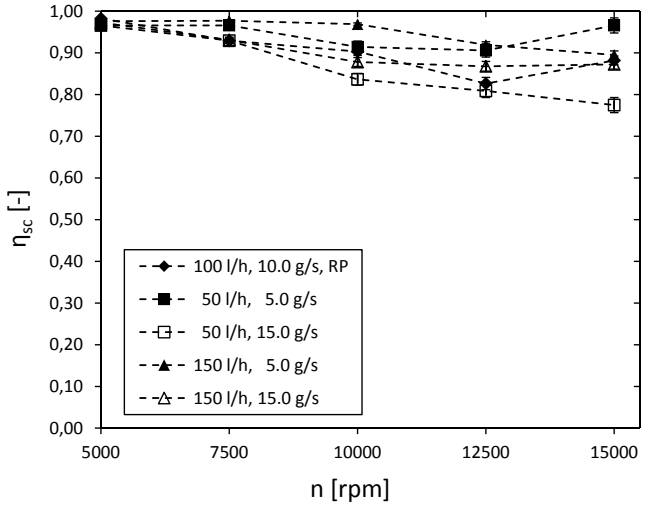

FIGURE 11. RAMP WITH 21° COVER: η_{sc} VS. SHAFT SPEED FOR DIFFERENT COMBINATIONS OF $\dot{V}_{l,in}$ AND $\dot{m}_{g,seal}$

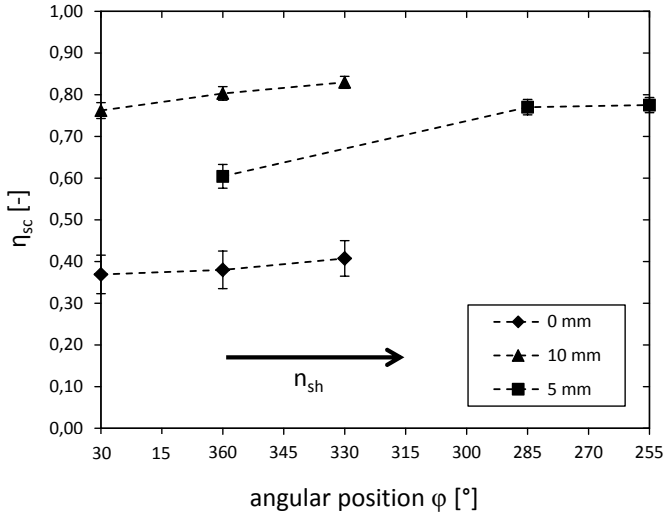

FIGURE 12. η_{sc} AT 15,000 rpm FOR DIFFERENT VENT PROTRUSION DEPTHS VS. VENT POSITION

respect to the rotor outer surface. Tests showed that a non-uniform seal clearance can result in either an increase or a decrease of the oil in the vent flow depending on the angular position of the maximum clearance height. Figure 13 shows the results for three cases: (1) the front cover was displaced by 0.2 mm to the left so that the maximum seal clearance of $h_{seal} = 0.9$ mm was at $\varphi = 270°$; (2) a uniform gap; (3) the front cover displaced to the right yielded a maximum clearance at $\varphi = 90°$. In the first case, with the maximum gap far from the vent offtake when seen in the direction of rotation, the scavenge efficiency generally decreased slightly. In the reverse case it increased. Although the

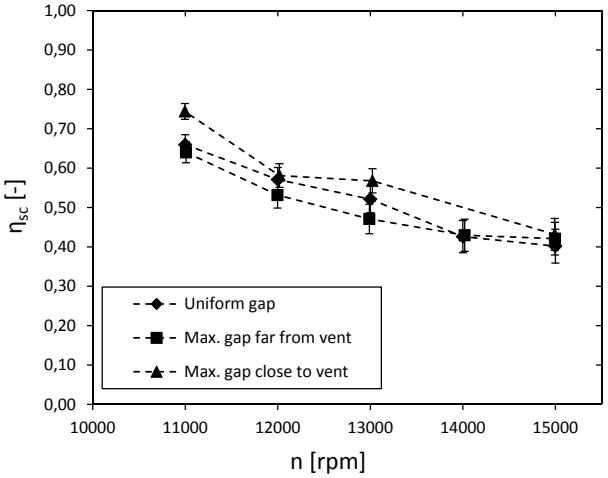

FIGURE 13. η_{sc} VS. SHAFT SPEED FOR UNIFORM AND NON-UNIFORM SEAL CLEARANCE; BASELINE OFFTAKES AT REFERENCE POINT CONDITIONS

deviations are within a few percent, this effect may be considered if the oil or secondary air system performance is different for two engines of the same type.

Film thickness

Oil film thickness measurements were taken with every operating point. As the protruding vent and the covered ramp were identified to have the highest impact on the oil split, these designs were compared to the baseline configuration in terms of the oil film distribution. Figures 14 - 16 show the averaged oil film thickness values $\overline{h_f}$ of the eight axially centered sensors at shaft speeds $n = 5,000$ rpm, 10,000 rpm and 15,000 rpm respectively. The arrow indicates the direction of the shaft surface velocity. The averaged angular distribution of the oil film at $n = 5,000$ rpm is shown in figure 14. At this low shaft speed, the offtake design has just as little influence on the oil film as it has on the scavenge efficiency. As gravity dominates the oil film flow, the film thickness increases towards the bottom ($\varphi = 180°$) of the chamber. At $n = 10,000$ rpm (figure 15) an improved oil separation of the covered ramp offtake can be detected as the film thickness values are clearly smaller than in the two other cases. The protruding vent offtake already slighty increases the level of the oil film compared to a flush vent. Finally, at $n = 15,000$ rpm the oil film distributions show significant differences between the different designs (figure 16). As the covered ramp efficiently collects the oil, a comparatively thin and more or less uniform oil film is measured in the chamber. Although a vent protruding 10 mm into the bearing chamber yields a scavenge efficiency close to the one of the covered ramp, the average oil film level is significantly higher. As the protruding vent prevents the oil from flowing out through the vent offtake, the instantaneous oil volume in

Copyright © 2012 by ASME

Downloaded From: http://proceedings.asmedigitalcollection.asme.org/pdfaccess.ashx?url=/data/conferences/asmep/74816/ on 05/01/2017 Terms of Use: http://www.asme.org/abo

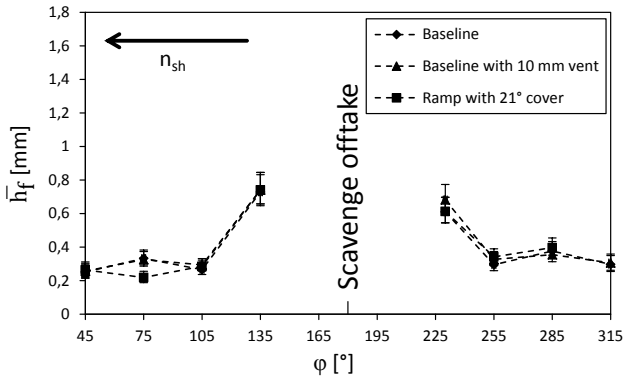

FIGURE 14. OIL FILM THICKNESS AT $n = 5,000$ rpm

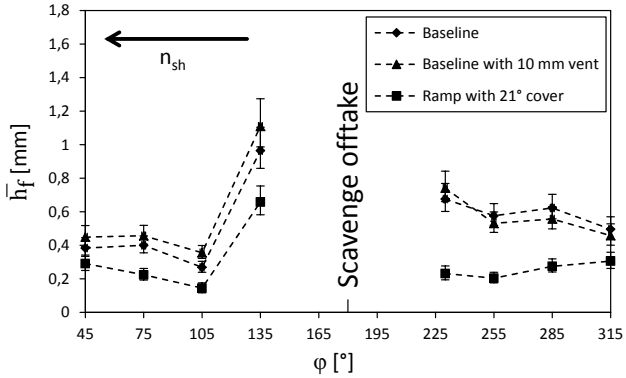

FIGURE 15. OIL FILM THICKNESS AT $n = 10,000$ rpm

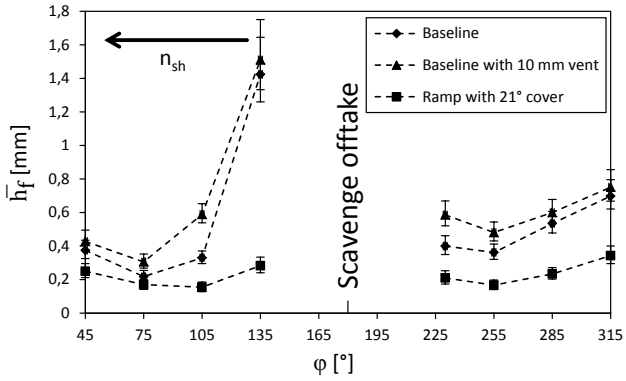

FIGURE 16. OIL FILM THICKNESS AT $n = 15,000$ rpm

the bearing chamber increases which in turn leads to higher oil film thicknesses.

CONCLUSIONS

An experimental investigation was performed to determine influences on the oil split between the two offtakes of a vented bearing chamber. First, a baseline bearing chamber configuration was examined at different operating conditions. Then, a systematic variation of a ramp scavenge offtake yielded that a covered ramp design increased the scavenge efficiency the most. With this design, the scavenge efficiency at 15,000 rpm was at a constantly high level of $77\,\% \leq \eta_{sc} \leq 97\,\%$ compared to a wide range of $21\,\% \leq \eta_{sc} \leq 56\,\%$ for the baseline configuration at the same operating conditions. A protruding vent was found as another measure to increase the scavenge efficiency significantly. Furthermore, a comparison of the baseline, the covered ramp scavenge and the protruding vent configuration showed a significant impact of each of the designs on the angular oil film thickness distribution. The covered ramp offtake proved to be the most efficient way to remove oil from the chamber. In addition, the effect of a non-uniform angular labyrinth seal clearance was examined. Due to the small nominal clearance, a small eccentricity between rotor and cover plate resulted in a non-uniform inflow of sealing air, which altered the scavenge efficiency by several percent.

The results show how the oil split and the oil distribution in the bearing chamber can actively be influenced by choosing a certain offtake design. Further investigations are necessary to identify the impact of other offtake designs and of other elements in a bearing chamber, such as oil jet blocks. Most important, however, is to extend the tests to different rotor diameters and different bearing chamber dimensions in order to render the results transferable to real engine applications.

ACKNOWLEDGMENT

The research leading to these results has received funding from the European Community's Seventh Framework Programme FP7/2007-2013 under grant agreement n°ACP8-GA-2009-233651.

REFERENCES

[1] Wittig, S., Glahn, A., and Himmelsbach, J., 1994. Influence of high rotational speeds on heat transfer and oil film thickness in aero engine bearing chambers. Journal for Gas Turbines and Power, Vol. 116, April 1994, Page 395-401.

[2] Glahn, A., and Wittig, S. K. L., 1996. Two-phase air/oil flow in aero engine bearing chambers - characterization of oil film flows. Journal of Engineering for Gas Turbines and Power, Vol. 118, July 1996, Page 578-583.

[3] Gorse, P., Busam, S., and Dullenkopf, K., 2006. Influence of operating condition and geometry on the oil film thickness in aero-engine bearing chambers. Journal of Engineer-

Copyright © 2012 by ASME

Downloaded From: http://proceedings.asmedigitalcollection.asme.org/pdfaccess.ashx?url=/data/conferences/asmep/74816/ on 05/01/2017 Terms of Use: http://www.asme.org/abo

ing for Gas Turbines and Power, Vol. 128, January 2006, Page 103-110.

[4] Glahn, A., and Wittig, S., 1996. Two-phase air/oil flow in aero engine bearing chambers- assessment of an analytical prediction method for the internal wall heat transfer. ISROMAC-6.

[5] Glahn, A., and Wittig, S., 1999. Two-phase air/oil flow in aero engine bearing chambers- assessment of an analytical prediction method for the internal wall heat transfer. International Journal of Rotating Machinery, Vol. 5, No. 3, Page 155-165.

[6] Busam, S., Glahn, A., and Wittig, S., 2000. Internal bearing chamber wall heat transfer as a function of operating conditions and chamber geometry. Journal of Engineering for Gas Turbines and Power, Vol. 122, April 2000, Page 314-320.

[7] Gorse, P., Dullenkopf, K., and Bauer, H.-J., 2005. The effect of airflow across aero-engine roller bearing on oil droplet generation. 17. ISABE.

[8] Gorse, P., Dullenkopf, K., Bauer, H.-J., and Wittig, S., 2008. An experimental study on droplet generation in bearing chambers caused by roller bearings. ASME-Paper GT2008-51281.

[9] Gorse, P., Willenborg, K., Busam, S., Ebner, J., Dullenkopf, K., and Wittig, S., 2003. Three-dimensional laser doppler anemometer(lda) measurements in an aero-engine bearing chamber. ASME-Paper GT2003-38376.

[10] Dagefoerde, H., Eastwick, C., Robinson, A., Johnson, G., Kontin, S., and Bauer, H.-J., 2008. Experimental investigation into the behaviour within flush offtake pipes. ASME-Paper GT2008-50632.

[11] Robinson, A., Morvan, H., and Eastwick, C., 2008. Computational investigations into aero-engine bearing chamber off-take flows. ASME-Paper GT2008-50634.

[12] Chandra, B., Pickering, S., Tittel, M., and Simmons, K., 2010. Factors affecting oil removal from an aeroengine bearing chamber. ASME-Paper GT2010-22631.

[13] Chandra, B., Simmons, K., Pickering, S., and Tittel, M., 2011. Liquid and gas flow behaviour in highly rotating environment. ASME-Paper GT2011-46430.

[14] Kurz, W., Dullenkopf, K., and Bauer, H.-J., 2011. The impact of geometry variations on the two-phase flows in aero-engine bearing chambers. 20. ISABE.

[15] Flouros, M., 2008. Analytical and numerical simulation of the two phase flow heat transfer in the vent and scavenge pipes of the clean engine demonstrator. ASME-Paper GT2008-50130.

[16] Robinson, A., Eastwick, C., and Morvan, H., 2010. Further computational investigations into aero-engine bearing chamber off-take flows. ASME-Paper GT2010-22626.

[17] Hashmi, A., Dullenkopf, K., Koch, R., and Bauer, H.-J., 2010. Cfd methods for shear driven liquid wall films. ASME-Paper GT2010-23532.

[18] Peduto, D., Hashmi, A., Dullenkopf, K., Bauer, H.-J., and Morvan, H., 2011. Modelling of an aero engine bearing chamber using enhanced cfd technique. ASME-Paper GT2011-45635.

[19] Wang, C., Morvan, H., Hibberd, S., and Cliffe, K., 2011. Thin film modelling for aero-engine bearing chambers. ASME-Paper GT2010-46259.

[20] Marshall, B., and Tiedermann, W., 1972. A capacitance depth gauge for thin liquid films. Rev. Sci. Instruments, Vol. 43, pp. 544-547.

[21] Kline, S. J., and McClintock, F. A., 1953. Describing uncertainties in single-sample experiments. Journal of Mechanical Engineering, Vol. 75, Nr. 1, Page 3-8.

Copyright © 2012 by ASME

Downloaded From: http://proceedings.asmedigitalcollection.asme.org/pdfaccess.ashx?url=/data/conferences/asmep/74816/ on 05/01/2017 Terms of Use: http://www.asme.org/abo